6272 *Chem. Mater.* **2010,** *22,* 6272–6279
DOI:10.1021/cm101814f

CHEMISTRY OF MATERIALS
Article

Synthesis of Silver Nanocubes in a Hydrophobic Binary Organic Solvent

Sheng Peng and Yugang Sun*

Center for Nanoscale Materials, Argonne National Laboratory, 9700 South Cass Avenue, Argonne, Illinois 60439, United States

Received June 29, 2010. Revised Manuscript Received September 28, 2010

Synthesis of metal nanoparticles with controlled shapes in hydrophobic solvents is challenging because homogeneous nucleation with high rate in these solvents is favorable for the formation of multiply twinned (MT) nanoparticles with spherical morphology. In this work, we report an inhomogeneous nucleation strategy in a binary hydrophobic solvent mediated by dimethyldistearylammonium chloride (DDAC), resulting in the coexistence of single-crystalline Ag polyhedrons and MT Ag quasi-spheres at the beginning of the reaction. In the consequent step, the MT Ag nanoparticles are selectively etched and dissolved through oxidation by NO_3^- ions (from the Ag precursor, $AgNO_3$) with the assistance of Cl^- ions (from DDAC). The dissolved Ag species are then reduced and deposited on the more stable single-crystalline polyhedrons to form Ag nanocubes. Synergy of the oxidative etching of MT particles and growth of single-crystalline particles leads to Ag nanocubes with high purity when the ripening time is long enough. For example, refluxing a mixing solvent of octyl ether and oleylamine containing $AgNO_3$ (0.02 M) and DDAC (0.03 M) at 260 °C for 1 h results in Ag nanocubes with an average edge length of 34 nm and a purity higher than 95%.

Introduction

Shape-controlled synthesis of metal nanoparticles represents an area attracting unprecedented interests in the past decade because of strong dependence of properties on their morphologies,[1−7] thus their performance in applications such as catalysis,[8−11] photonics,[12−15] imaging,[16−18] sensing,[19−21] energy,[22−25] and medicine.[16,26−28] For example, cubic Ag nanoparticles bounded with {100} facets exhibit much higher catalytic capability toward oxidation of styrene with *tert*-butyl hydroperoxide than Ag nanoplates mainly bounded with {111} facets.[29] Here, we are interested in the synthesis of Ag nanocubes in hydrophobic solvents. Extensive efforts have been devoted to understanding the growth mechanism in the formation of single-crystalline Ag nanocubes since the successful synthesis of Ag nanocubes by Sun and Xia through a polyol reduction of silver nitrate ($AgNO_3$) in ethylene glycol with assistance of poly(vinyl pyrrolidone) (PVP).[30] For instance, Ag nanocubes with improved quality in terms of yield, purity, and uniformity have been synthesized in hydrophilic solvents (e.g., ethylene glycol, water, etc.) through oxidative etching with dissolved oxygen to selectively eliminate multiply twinned (MT) nanoparticles in the presence of anions (for example, chloride

*Corresponding author. E-mail: ygsun@anl.gov.

(1) Burda, C.; Chen, X.; Narayanan, R.; El-Sayed, M. A. *Chem. Rev.* **2005**, *105*, 1025–1102.
(2) Xia, Y.; Xiong, Y.; Lim, B.; Skrabalak, S. E. *Angew. Chem., Int. Ed.* **2009**, *48*, 60–103.
(3) Jin, R.; Cao, Y. C.; Hao, E.; Métraux, G. S.; Schatz, G. C.; Mirkin, C. A. *Nature* **2003**, *425*, 487–490.
(4) Murphy, C. J.; Gole, A. M.; Hunyadi, S. E.; Orendorff, C. J. *Inorg. Chem.* **2006**, *45*, 7544–7554.
(5) Tao, A. R.; Habas, S.; Yang, P. *Small* **2008**, *4*, 310–325.
(6) Zhang, Q.; Ge, J.; Pham, T.; Goebl, J.; Hu, Y.; Lu, Z.; Yin, Y. *Angew. Chem., Int. Ed.* **2009**, *48*, 3516–3519.
(7) Sohn, K.; Kim, F.; Pradel, K. C.; Wu, J.; Peng, Y.; Zhou, F.; Huang, J. *ACS Nano* **2009**, *3*, 2191–2198.
(8) Narayanan, R.; El-Sayed, M. A. *Nano Lett.* **2004**, *4*, 1343–1348.
(9) Tian, N.; Zhou, Z.-Y.; Sun, S.-G.; Ding, Y.; Wang, Z. L. *Science* **2007**, *316*, 732–735.
(10) Lim, B.; Jiang, M.; Camargo, P. H. C.; Cho, E. C.; Tao, J.; Lu, X.; Zhu, Y.; Xia, Y. *Science* **2009**, *324*, 1302–1305.
(11) Peng, Z.; You, H.; Wu, J.; Yang, H. *Nano Lett.* **2010**, *10*, 1492–1496.
(12) Maier, S. A.; Kik, P. G.; Atwater, H. A. *Appl. Phys. Lett.* **2002**, *81*, 1714–1716.
(13) Guo, X.; Qiu, M.; Bao, J.; Wiley, B. J.; Yang, Q.; Zhang, X.; Ma, Y.; Yu, H.; Tong, L. *Nano Lett.* **2009**, *9*, 4515–4519.
(14) Yan, R.; Pausauskie, P.; Huang, J.; Yang, P. *Proc. Natl. Acad. Sci. U.S.A.* **2009**, *106*, 21045–21050.
(15) Gansel, J. K.; Thiel, M.; Rill, M. S.; Decker, M.; Bade, K.; Saile, V.; von Freymann, G.; Linden, S.; Wegener, M. *Science* **2009**, *325*, 1513–1515.
(16) Jain, P. K.; Lee, K. S.; El-Sayed, I. H.; El-Sayed, M. A. *J. Phys. Chem. B* **2006**, *110*, 7238–7248.
(17) Murphy, C. J.; Gole, A. M.; Stone, J. W.; Sisco, P. N.; Alkilany, A. M.; Goldsmith, E. C.; Baxter, S. C. *Acc. Chem. Res.* **2008**, *41*, 1721–1730.
(18) Chen, J.; Saeki, F.; Wiley, B. J.; Cang, H.; Cobb, M. J.; Li, Z.-Y.; Au, L.; Zhang, H.; Kimmey, M. B.; Li, X.; Xia, Y. *Nano Lett.* **2005**, *5*, 473–477.
(19) Banholzer, M. J.; Millstone, J. E.; Qin, L.; Mirkin, C. A. *Chem. Soc. Rev.* **2008**, *37*, 885–897.
(20) Sherry, L. J.; Jin, R.; Mirkin, C. A.; Schatz, G. C.; Van Duyne, R. P. *Nano Lett.* **2006**, *6*, 2060–2065.
(21) Tao, A.; Kim, F.; Hess, C.; Goldberger, J.; He, R.; Sun, Y.; Xia, Y.; Yang, P. *Nano Lett.* **2003**, *3*, 1229–1233.
(22) Atwater, H. A.; Polman, A. *Nat. Mater.* **2010**, *9*, 205–213.
(23) Kulkarni, A. P.; Noone, K. M.; Munechika, K.; Guyer, S. R.; Ginger, D. S. *Nano Lett.* **2010**, *10*, 1501–1505.
(24) Standridge, S. D.; Schatz, G. C.; Hupp, J. T. *J. Am. Chem. Soc.* **2009**, *131*, 8407–8409.
(25) Tian, Y.; Tatsuma, T. *J. Am. Chem. Soc.* **2005**, *127*, 7632–7637.
(26) Chen, J.; Glaus, C.; Laforest, R.; Zhang, Q.; Yang, M.; Gidding, M.; Welch, M. J.; Xia, Y. *Small* **2010**, *6*, 811–817.
(27) Lal, S.; Clare, S. E.; Halas, N. J. *Acc. Chem. Res.* **2008**, *41*, 1842–1851.
(28) Zhang, J. Z. *J. Phys. Chem. Lett.* **2010**, *1*, 686–695.
(29) Xu, R.; Wang, D.; Zhang, J.; Li, Y. *Chem. Asian J.* **2006**, *1*, 888–893.
(30) Sun, Y.; Xia, Y. *Science* **2002**, *298*, 2176–2179.

Published on Web 11/15/2010

from HCl,[31] $CuCl_2$,[32] NaCl;[33] bromide from CTAB;[34] and sulfide from Na_2S,[35] NaHS[35,36]) that can coordinate with Ag^+ ions to effectively promote the oxidation of twinned nanoparticles. However, this strategy faces difficulty to extend to the synthesis of Ag nanocubes in hydrophobic organic solvents because of the low solubility of the aforementioned halogenide and chalcogenide compounds in these solvents. During preparation of the current paper, we noticed a most recent report from Xia's group describing the synthesis of Ag nanocubes in a hydrophobic solvent (i.e., a mixture of isoamyl ether and oleylamine) by adding trace amount of $FeCl_3$ (or $Fe(acac)_3$), which synergistically works with dissolved oxygen in the solvent to selectively etch MT Ag nanoparticles.[37] The advantages for synthesizing metal nanoparticles in a hydrophobic solvent include high yield, narrow size distribution, and ease in assembly of them into superlattices.[38−42] Herein, we present an alternative method for the synthesis of Ag nanocubes in a binary hydrophobic solvent containing octyl ether (OE) and oleylamine (OAm) through reduction of $AgNO_3$ at high temperature with the assistance of dimethyldistearylammonium chloride (DDAC). The amphiphilic DDAC molecules are well dissolved in the binary solvent to release Cl^- ions that play important roles in (i) precipitation with Ag^+ ions in the formation of single-crystalline AgCl nanoparticles that are further reduced to single crystalline Ag nanoparticles; and (ii) selective etching of MT Ag nanoparticles with oxidative species such as NO_3^- ions to grow the single crystalline Ag nanoparticles into Ag nanocubes. The resulting Ag nanocubes exhibit a very high yield (> 90%), narrow size distribution (< 10%), and high purity in cubic morphology (> 95%).

Experimental Section

Materials. Octyl ether (OE, 99%) and dimethyldistearylammonium chloride (DDAC, > 97%), and oleylamine (OAm, assay 70%, primary amine > 98%, Lot#BCBB4159) were purchased from Sigma-Aldrich (Milwaukee, WI). Silver nitrate ($AgNO_3$, 99.9%) was purchased from STREM chemicals (Newburyport, MA). Hexane (Mallinckrodt, AR*ACS grade) was purchased from VWR International (West Chester, PA). All chemicals were received and used without further purification.

Synthesis of Ag Nanocubes. In a typical synthesis, 8.0 mL of OE and 1.0 mL of OAm were sequentially added to a 50 mL three-neck flask connected to a Schlenk line that was purged with nitrogen. DDAC powder (0.176 g (0.3 mmol)) was then added to the binary solvent (OE-OAm) under magnetic stirring. Heating the solvent to 60 °C by placing the flask on a heating mantle that was controlled by a digital thermal controller and maintaining the temperature for 10 min completely dissolved DDAC. The resulting colorless solution was then quickly heated up to 260 °C at a ramp rate of ~10 °C/min with the same heating mantle. Once the temperature was stabilized at 260 °C, 1.0 mL of an OAm solution of $AgNO_3$ (0.2 M) that was preheated at 50 °C was quickly injected into the flask with a syringe. The reaction solution instantaneously turned milky yellowish and then deep yellow within 1 min. Maintaining the reaction at 260 °C for 1 h completed the synthesis of Ag nanocubes. Then the reaction solution was quickly cooled down to room temperature within 5 min by removing the heating mantle and blowing air to the surface of the reaction flask. Nitrogen purging and magnetic stirring (~600 rpm) were maintained throughout the entire synthesis. A small proportion (0.5−1 mL) of the resulting solution was gently centrifuged at a rate of 2000 rpm (300 *g*) for 30 s with a microcentrifuge (Galaxy 14D centrifuge, VWR) to collect the Ag nanocubes, which were then redispersed in hexane. Such a process was repeated additional times if necessary. The rotation rate applied to the different cycles was the same throughout the washing processes which primarily remove the free molecules of DDAC, OAm, and OE. Transmission electron microscopy (TEM) observations indicate that self-assembly behavior of the Ag nanocubes on TEM grids was not influenced after the samples were washed for different times. Control experiments were carried out through the same process except the difference of the parameters mentioned in the following sections.

As for the time-dependent study, small aliquots (~0.5 mL) of reaction solution were taken out from the flask at different reaction times (normalized against the time at which the solution of $AgNO_3$ was injected into the binary solvent) using a glass syringe with a stainless steel needle, which was preheated over the hot reaction solution for 5 min to minimize the effect of temperature fluctuation caused by immersing the syringe needle in the reaction solution. The hot solutions were immediately transferred to glass vials (3 mL), which had been buried in ice to quickly quench possible reactions. The cooled solutions were then centrifuged followed by washing and redispersing with hexane.

Characterization. Samples for TEM analysis were prepared by putting droplets of hexane dispersions of the as-synthesized Ag nanoparticles on copper grids coated with thin amorphous carbon films (Ted Pella, Inc.). The samples were then dried in a fume hood at room temperature. TEM images were taken on a Philips CM30 with an acceleration voltage of 200 kV. High resolution TEM (HRTEM) images were taken on an FEI Tecnai F20ST TEM/STEM with an acceleration voltage of 200 kV. Energy-dispersive X-ray spectroscopy (EDS) and high-angle annular dark field scanning TEM (HAADF-STEM) images were obtained on a JEOL 2010F (S)TEM with an acceleration voltage of 200 kV. UV−visible extinction spectra were measured with a Varian Cary 50 Scan spectrometer by loading the reaction solutions in a quartz cuvette with 1 cm light path length. X-ray diffraction (XRD) patterns were acquired by a Bruker D8 Advanced Diffractometer with Cu Kα (1.5406 Å) source. To

(31) Im, S. H.; Lee, Y. T.; Wiley, B.; Xia, Y. *Angew. Chem., Int. Ed.* **2005**, *44*, 2154–2157.
(32) Tao, A.; Sinsermsuksakul, P.; Yang, P. *Angew. Chem., Int. Ed.* **2006**, *45*, 4597–4601.
(33) Wiley, B.; Herricks, T.; Sun., Y.; Xia, Y. *Nano Lett.* **2004**, *4*, 1733–1739.
(34) Yu, D.; Yam, V. W.-W. *J. Am. Chem. Soc.* **2004**, *126*, 13200–13201.
(35) Siekkinen, A. R.; McLellan, J. M.; Chen, J.; Xia, Y. *Chem. Phys. Lett.* **2006**, *432*, 491–496.
(36) Zhang, Q.; Cobley, C. M.; Au, L.; McKiernan, M.; Schwartz, A.; Chen, J.; Wen, L.; Xia, Y. *ACS Appl. Mater. Interfaces* **2009**, *1*, 2044–2048.
(37) Ma, Y.; Li, W.; Zeng, J.; McKiernan, M.; Xie, Z.; Xia, Y. *J. Mater. Chem.* **2010**, *20*, 3586–3589.
(38) Lin, X. Z.; Teng, X.; Yang, H. *Langmuir* **2003**, *19*, 10081–10085.
(39) Peng, S.; Wang, C.; Xie, J.; Sun, S. *J. Am. Chem. Soc.* **2004**, *128*, 10676–10677.
(40) Shevchenko, E. V.; Talapin, D. V.; Rogach, A. L.; Kornowski, A.; Haase, M.; Weller, H. *J. Am. Chem. Soc.* **2002**, *124*, 11480–11485.
(41) Zheng, N; Fan, J; Stucky, G. D. *J. Am. Chem. Soc.* **2006**, *128*, 6550–6551.
(42) Shevchenko, E. V.; Talapin, D. V.; Kotov, N. A.; O'Brien, S.; Murray, C. B. *Nature* **2006**, *439*, 55–59.

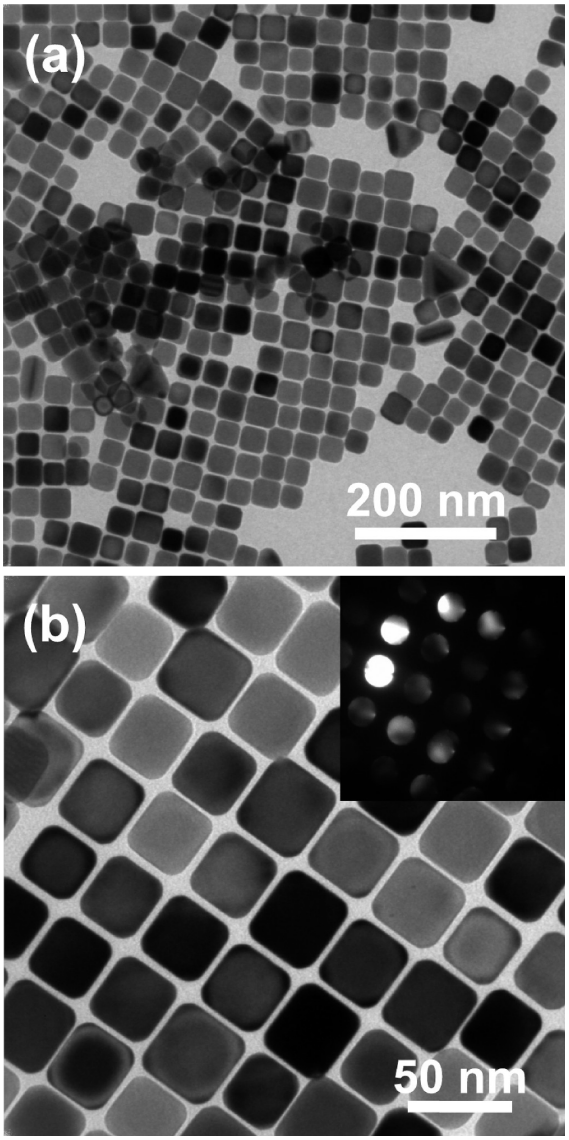

Figure 1. (a) Low- and (b) high-magnification TEM images of the as-synthesized Ag nanocubes. Inset in b shows convergent beam electron diffraction pattern of an individual nanocube. Reaction conditions were described in the Experimental Section.

prepare the samples for XRD study, we suspended the washed nanocubes (~5 mg) in a small volume of acetone (~0.1 mL), and then drop-cast onto removable double-sided tape (Scotch tape, polyester carrier/acrylic adhesive, 3M). Acetone quickly evaporated, resulting in a circular thin film of dried particles with a diameter of ~5 mm. The film was then sealed with another layer of tape, and the sealed film was adhered to the sample stage.

Results and Discussion

The typical synthesis described in the Experimental Section leads to a product of Ag nanocubes with high purity. Figure 1 presents typical TEM images of the as-synthesized nanoparticles, clearly showing their cubic morphology with slight truncation and uniform size with edge length of 34.0 ± 2.9 nm (standard deviation of 8.5%). TEM images obtained by tilting the nanoparticles at different degrees confirm they are cubes rather than square-like plates (see the Supporting Information, Figure S1).

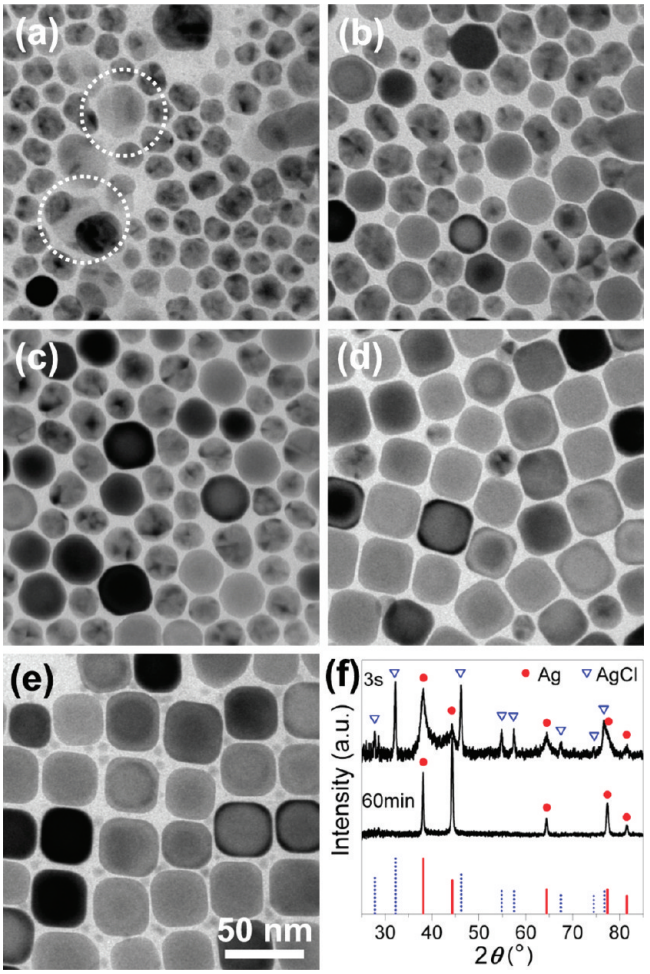

Figure 2. (a–e) TEM images of the samples formed at various times after the injection of $AgNO_3$ solution into the hot OE-OAm solution of DDAC: (a) 3 s, (b) 1 min, (c) 5 min, (d) 10 min, and (e) 30 min. The scale bar in (e) applies to (a–e). Other reaction conditions are the same as those of Figure 1. (f) XRD patterns of the samples formed at 3 s (top curve, corresponding to the nanoparticles shown in a) and 60 min (bottom curve, corresponding to the nanoparticles shown in Figure 1). Diffraction peaks from Ag and AgCl are marked with red solid circles and blue hollow triangles, respectively. Standard patterns of Ag (red solid peak-sticks, ICDD PDF No. 04–001–3180) and AgCl (blue dotted peak-sticks, ICDD PDF No. 04–006–5535) are included for comparison. The intensity ratio between the (200) and (111) peaks for the sample formed at 60 min (bottom curve) is 1.55, which is exceptionally higher than the ratio (i.e., 0.4) for conventional Ag powders. The increased intensity of the (200) peak is ascribed to that the Ag nanocubes are mainly bounded by {100} facets and they tend to stand on the substrate against the flat {100} surfaces.

X-ray diffraction (XRD, Figure 2f) pattern and energy-dispersive X-ray spectroscopy (EDS) of the as-synthesized nanocubes indicate they are composed of pure Ag with face-centered cubic (fcc) phase. Each Ag nanocube exhibits highly uniform contrast in the TEM images, indicating the nanoparticles are free of twin defects. The single square symmetry of the convergent beam electron diffraction pattern (inset of Figure 1b) that is obtained by aligning the electron beam perpendicular to one of the six surfaces of an individual Ag nanocube and its high-resolution TEM (HRTEM) image (see the Supporting Information, Figure S2) further confirm that each nanocube is a single crystal with its surfaces bounded by {100} facets. Statistical studies indicate that the products synthesized

through the present approach contain more than 95% of Ag nanocubes and a very low percentage of nanoparticles with other morphologies such as rods and tetrahedrons. The Ag nanocubes have a great tendency to self-assemble into two-dimensional ordered superlattices (Figure 1) when the TEM samples are prepared by drying the hexane dispersion of Ag nanocubes in ambient environment, clearly showing the potential feasibility to use the Ag nanocubes synthesized in the hydrophobic solvents as building blocks for fabrication of superlattices with complex architectures.[42]

Time-Dependent Evolution of Ag Nanocubes. The evolution of Ag nanocubes involved in the synthetic reaction has been monitored by TEM and XRD characterization over the products formed at different times after the injection of $AgNO_3$ into the reaction solution. Figure 2 compares the morphologies and crystalline phases of the nanoparticles formed at different reaction stages, clearly showing the gradual disappearance of MT nanoparticles and increase in the population of nanocubes as elongation of the reaction time. Once the OAm solution of $AgNO_3$ is swiftly injected to the solution of DDAC, the reaction solution immediately becomes milky yellowish (see the Supporting Information, Figure S3a) because of the simultaneous formation of AgCl nanoparticles that are precipitated through reaction of Ag^+ and Cl^- ions and Ag nanoparticles that are generated through reduction of $AgNO_3$ with OAm. The free Cl^- ions are generated from the dissociation of DDAC under the reaction conditions. DDAC is a quaternary ammonium compound composed of permanently charged quaternary ammonium cations and counter Cl^- anions and is in the form of ion-pairs in solid state. In contrast, the ion-pairs can dissociate in solvents at elevated temperatures to promote the release of free Cl^- ions that can be used to mediate nanoparticle synthesis. For instance, DDAC has recently been used as a source of Cl^- ions in mediating structural transformation of zinc blende CdS nanoparticles to wurtzite pencil-like nanorods at 260 °C.[43] In general, AgCl nanoparticles in dispersion exhibit milky color due to their large band gaps[44] and Ag nanoparticles exhibit strong optical absorption in blue due to their surface plasmon resonance (SPR).[45] Extinction spectrum (see the Supporting Information, Figure S4) of the sample formed at 3 s clearly shows a distinct peak at ~320 nm (corresponding to the absorption of AgCl nanoparticles) with a broad tail in the range of 400−600 nm (corresponding to the SPR of Ag nanoparticles). Figure 2a presents a TEM image of the milky yellow product formed at the very early stage (i.e., 3 s), clearly showing the coexistence of nanoparticles with bimodal sizes, i.e., 10−15 nm and ~30 nm. EDS analysis on an assembly of many nanoparticles over an area of ~1 μm^2 on a TEM grid shows the nanoparticle product contains an average of ~20% Cl (atomic ratio) (see the Supporting Information, Figure S5a). This value is underestimated because of the loss of Cl caused by quick reduction of AgCl that is exposed to the electron beam during the period (i.e., ~60 s) of spectral acquisition. Nevertheless, it is no doubt that the AgCl nanoparticles exist in the early product. Under irradiation of electron beam in the TEM chamber, only the larger particles (highlighted with white dotted circles) are not stable, indicating that they are composed of AgCl. On the other hand, the smaller nanoparticles are stable under electron irradiation, confirming that they are composed of pure Ag. We attempted to conduct elemental mapping and line-profiling analyses on individual nanoparticles with the use of EDS. Unfortunately, exposure of the AgCl nanoparticles to the electron beam immediately reduces AgCl to Ag, leading to morphological and compositional change of the AgCl nanoparticles. High-angle annular dark field scanning transmission electron microscopy (HAADF-STEM) images (see the Supporting Information, Figure S6) of this sample clearly show the instability of the AgCl nanoparticles under the electron beam. The AgCl nanoparticles can be partially reduced to form elemental Ag domains in the AgCl nanoparticles even the sample is exposed to the electron beam for a very short period (< 1s) that is required for taking an image (see the Supporting Information, Figure S6a). As a result, elemental mapping based on EDS that usually takes long acquiring time (e.g., several minutes to several hours) is not practical to identify the AgCl nanoparticles and Ag nanoparticles. Instead, we compared the HAADF-STEM images (see the Supporting Information, Figure S6) and the spot EDS analysis (see the Supporting Information, Figure S7a). The comparison differentiates Ag nanoparticles (i.e., smaller spherical particles with brighter contrast in STEM images) and AgCl nanoparticles (i.e., large cubic particles with grayer contrast in STEM images) in this sample. In addition, XRD pattern of the sample exhibits strong peaks of both AgCl and Ag (top curve of Figure 2f). The widths of Ag peaks are much broader than those of AgCl peaks, confirming that the larger particles in the sample correspond to AgCl and the smaller ones to Ag. Mean sizes of the crystalline domains of AgCl and Ag are estimated from the XRD pattern to be ~25 and ~6 nm, respectively, according to the Scherrer's equation. The calculated value for the AgCl nanoparticles is comparable to their average size of ~30 nm (versus ~25 nm) evaluated from TEM images, whereas the calculated value for the Ag nanoparticles is much smaller than their average size of ~15 nm (versus ~6 nm). These results are consistent with the single crystallinity (i.e., crystalline domain size equals to nanoparticle size) of the AgCl nanoparticles and MT crystallinity (i.e., crystalline domain size is smaller than nanoparticle size) of the Ag nanoparticles.

The AgCl particles can be quickly reduced to Ag by OAm at high temperatures, resulting in that the milky yellow color disappears and the reaction solution becomes very deep yellow (see the Supporting Information, Figure S3b). This color variation is consistent with the difference

(43) Saruyama, M.; Kanehara, M.; Teranishi, T. *J. Am. Chem. Soc.* **2010**, *132*, 3280–3282.
(44) Glaus., S.; Galzaferri, G. *Photochem. Photobiol. Sci.* **2003**, *2*, 398–401.
(45) Kelly, K. L.; Coronado, E.; Zhao, L. L.; Schatz, G. C. *J. Phys. Chem. B* **2003**, *107*, 668–677.

between the extinction spectra of the samples formed at 3 s and 1 min, i.e., the peak at ~320 nm disappears while a new distinct peak at ~420 nm emerges with increase of the reaction time (see the Supporting Information, Figure S4, black curve vs blue curve). The sample obtained at 1 min is essentially composed of pure Ag, as reflected by the XRD pattern and EDS spectra (see the Supporting Information, Figures S5b and S7c). TEM image (Figure 2b) of this sample also shows bimodal size distribution similar to the sample obtained at 3 s (Figure 2a), i.e., the smaller ones with MT structures and the larger one with single crystallinity. However, the larger nanoparticles are stable under illumination of electron beam, indicating that the single crystalline AgCl nanoparticles shown in Figure 2a have been converted to single-crystalline Ag nanoparticles through reduction by OAm. Most of them exhibit polyhedral morphologies, such as cuboctahedron, truncated cube, etc., which are corresponding to the hexagonal projection profiles in the TEM image. The mechanism involved in the chemical transformation and structural retaining is not clear and needs to be explored. Meanwhile, the size of the MT Ag nanoparticles slightly increases possibly because of the continuous reduction of Ag^+ ions by OAm. Once the Ag^+ ions are completely reduced, the growth of MT nanoparticles stops. For example, the MT nanoparticles in the sample formed at 5 min do not show a size increase in comparison with those formed at 1 min (Figure 2c vs Figure 2b), instead, their size slightly decreases. In contrast, the single crystalline polyhedral particles slightly increase in size and most of them become truncated cubes. The different trends in size change for the single-crystalline particles and the MT ones indicate that the continuous growth of single-crystalline nanoparticles is beneficial from the dissolution of the MT particles. The difference is more clearly shown in panels d and e of Figure 2, in which the size and population of the MT particles dramatically decrease and the single-crystalline particles become nanocubes with slightly rounded corners for the samples formed at 10 and 30 min. When the ripening time is long enough (e.g., 60 min), the MT nanoparticles are completely dissolved, resulting in the formation of monodisperse Ag nanocubes with high purity (Figure 1). Mean size of crystalline domain of the Ag nanocubes calculated from the XRD pattern (Figure 2f, bottom curve) is ~28 nm that is comparable to their average size of ~34 nm evaluated from the TEM images, indicating that each Ag nanocube is crystallized as a single crystal.

Effect of Concentration of DDAC. The results shown in Figure 2 indicate that addition of DDAC molecules that provide free Cl^- ions is important for the growth of high-quality Ag nanocubes because the single crystalline seeds originate from the single crystalline AgCl nanoparticles. If the reaction is free of DDAC, injection of OAm solution of $AgNO_3$ to the OE-OAm binary solvent instantaneously results in a yellow color, indicating that the solvent itself reduce Ag^+ ions to form Ag nanoparticles with high rate at high temperature. The final product contains only spherical MT nanoparticles with sizes around 10 nm (Figure 3a). The absence of single-crystalline nanoparticles in Figure 3a confirms the importance of AgCl nanoparticles in the formation of single-crystalline Ag nanocubes. When DDAC (even with low concentration of 0.01 M, i.e., one-third of the concentration used in the synthesis of the sample shown in Figure 1) is introduced to the reaction system, the resulting nanoparticles (Figure 3b) exhibit significant difference in size and crystallinity from those synthesized without DDAC (Figure 3a). Most nanoparticles have sizes larger than 30 nm and the product contains Ag nanocubes (30% in population) along nanoparticles with other morphologies and twinning defects (highlighted with white dotted circles) (Figure 3b). Smaller MT nanoparticles with sizes of ~10 nm are not observed in this sample. Increasing the concentration of DDAC to 0.03 M results in Ag nanocubes with high purity (>95%), with complete elimination of twinned nanoparticles (Figure 1). The difference of samples shown in Figures 3b, 1, and 2

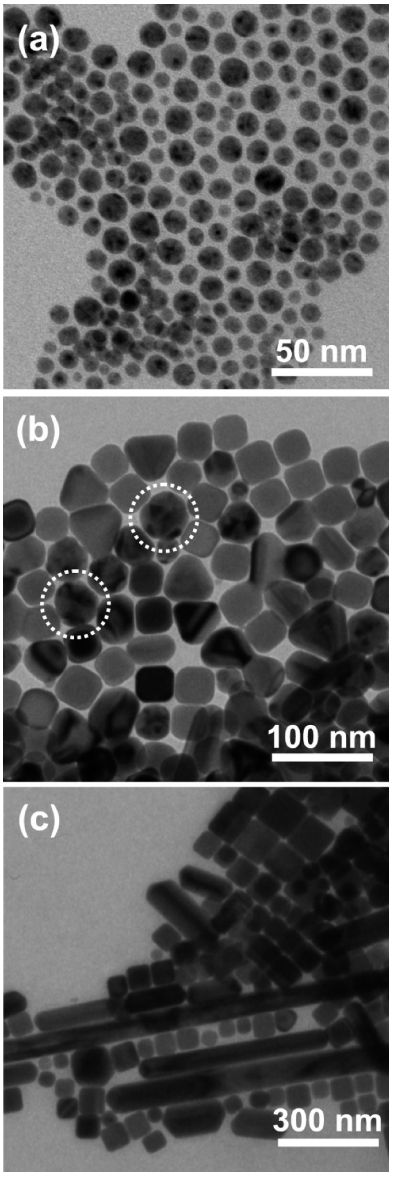

Figure 3. TEM images of Ag nanoparticles synthesized from reactions performed in the presence of DDAC with different concentrations: (a) 0, (b) 0.01, and (c) 0.10 M. Other reaction conditions were the same as those of Figure 1.

indicates that DDAC also facilitates the etching of MT particles to continuously grow the single-crystalline nanoparticles into Ag nanocubes. It is well-known that Ag nanoparticles with MT defects are easier than single crystalline Ag nanoparticles to be etched through oxidation reaction with oxygen in the presence of Cl^- ions, which coordinate with the resulting Ag^+ ions.[33] By carefully examining the present reaction system, oxidative etching of MT Ag nanoparticles may be driven by NO_3^- ions (and/or their derivatives) with assistance of Cl^- ions. Although nitrate ions, in general, have negligible oxidative capability in neutral or basic solutions, slightly increasing the acidity of solutions can drastically enhance their oxidizability. Under the reaction conditions for the synthesis of the sample shown in Figure 1, additional H^+ ions may be generated from the following reactions: (i) hydrolysis of DDAC at high temperatures with the trace amount of water existing in the OE-OAm solvent and hygroscopic DDAC powders, and (ii) reduction of Ag^+ ions with OAm molecules because of the dehydrogenation of amines and formation of C=N and C≡N bonds.[46] In addition, the species derived from the reduction of NO_3^- ions (with OAm), e.g., NO_2 and N_2O, can exhibit even stronger oxidizability. On the other hand, replacing $AgNO_3$ with silver trifluoroacetate ($AgCF_3COO$), whose anions do not have oxidative capability, results in a mixture of single-crystalline and MT nanoparticles. In this case, the initial AgCl nanoparticles are reduced by OAm to form single-crystalline Ag nanoparticles, whereas the MT Ag ones cannot be completely etched with only Cl^- ions. Such experiments confirm the role of NO_3^- ions and their derivatives in etching MT nanoparticles. However, much higher concentration of DDAC (0.1 M) leads to the formation of Ag nanocubes with larger sizes (~60−120 nm) along with polydispersed nanorods (Figure 3c). This might be ascribed to that higher concentration of Cl^- ions induces higher etching power that etches single-crystalline Ag nanocubes to further enlarge the more stable nanocubes in either isotropic or anisotropic mode. As a result, the Cl^- ions derived from DDAC molecules play important roles for the formation of Ag nanocubes in two sequential steps: (i) they react with Ag^+ ions to form AgCl nanoparticles followed by reduction with OAm, resulting in single-crystalline Ag polyhedrons; (ii) they accelerate the oxidative etching (and dissolution) of MT Ag nanoparticles by NO_3^- ions (and their derivatives), followed by reduction with OAm to enlarge the stable single-crystalline polyhedrons into Ag nanocubes. In the latter process, Ag^+ ions generated from the etching of MT Ag nanoparticles do not form AgCl precipitate before they are reduced back to Ag atoms that are condensed on the single crystalline Ag nanoparticles. This argument is supported by the following facts: (i) the etching process of the MT Ag nanoparticles occurs at high temperatures (e.g., 260 °C), at which the solubility of AgCl is significantly

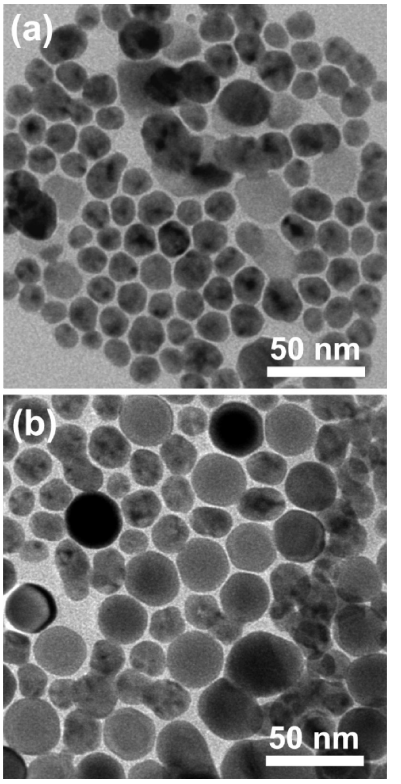

Figure 4. TEM images of nanoparticles synthesized at different temperatures: (a) 180 and (b) 220 °C. Other reaction conditions were the same as those of Figure 1.

increased in comparison with that at room temperature;[47] (ii) the low concentration Ag^+ ions may form soluble $AgCl_2^-$, $AgCl_3^{2-}$, or $AgCl_4^{3-}$ complex ions rather than solid AgCl because of the existence of high-concentration Cl^- ions;[48,49] and (iii) the strong reducing ability of OAm at high temperatures and structural stability of the single-crystalline Ag nanoparticles can facilitate the quick reduction of soluble Ag species to grow the single-crystalline Ag nanoparticles into Ag nanocubes. In addition, the time-dependent extinction spectra (see the Supporting Information, Figure S4) of the samples formed during the synthesis do not show the formation of AgCl during the dissolution of MT Ag nanoparticles (i.e., reaction time > 1 min).

Effect of Composition of the Binary Solvent. In the current reaction system, OE may help the binary solvent better dissolve the DDAC molecules to release a high concentration of Cl^- ions at elevated temperatures to drive the aforementioned reactions (described in the previous section) for the growth of Ag nanocubes. If the solvent is composed of pure OAm (i.e., no OE), the reaction leads to the formation of Ag nanoparticles with a very wide size distribution (see the Supporting Information, Figure S8a). Essentially all the particles contain twin defects, indicating that the twinned nanoparticles cannot be etched when the concentration of Cl^- ions is very low. Substituting OE with benzyl ether (BE), which is composed of benzyl groups that interact weakly with DDAC molecules, also

(46) Chen, M.; Feng, Y.-G.; Wang, X.; Li, T.-C.; Zhang, J.-Y.; Qian, D.-J. *Langmuir* **2007**, *23*, 5296–5304.
(47) Lide, D. R., Ed. *CRC Handbook of Chemistry and Physics*, 84th ed.; CRC Press: Boca Raton, FL, 2003.
(48) Tumidajski, P. J.; Blander, M.; Newman, D. S. *J. Electrochem. Soc.* **1994**, *141*, 895–900.
(49) Zelyanskii, A. V.; Zhukova, L. V.; Kitaev, G. A. *Inorg. Mater.* **2001**, *37*, 523–526.

results in poor solubility of DDAC, leading to the difficulty for growing Ag nanocubes. The oxidative capability of "O" in OE molecules is negligible for oxidative etching of MT Ag nanoparticles because replacing OE with 1-octadecene (OD) does not significantly influence the quality of Ag nanocubes. On the other hand, OAm acts as both a reducing agent with reducing ability increased at elevated temperatures and a surfactant for stabilizing the resulting Ag nanoparticles. For example, a control synthesis performed by injecting 0.4 mL of an OAm solution of $AgNO_3$ (0.5 M) into a hot solution of 9.6 mL of OE containing 0.3 mmol of DDAC. The binary solvent contains 96% OE in volume ratio and only 4% OAm. The reaction leads to the formation of Ag nanoparticles with a wide range of sizes and morphologies although most of them are single-crystalline (see the Supporting Information, Figure S8b). The poor morphological and dimensional control on the Ag nanoparticles indicates that OAm with high concentration is important to serve as surfactant for assisting growth of the Ag nanoparticles with high uniformity.[50] In addition, the Ag nanoparticles accumulate on the wall of reaction flask to form a Ag mirror during reaction, implying high concentration OAm is also necessary to prevent the Ag nanoparticles from aggregation. Therefore, tuning the composition of the binary solvent to balance the etching capability of NO_3^- ions medicated by Cl^- ions and reducing ability/surfactant capping ability of OAm is critical for the formation of Ag nanocubes with high purity through elimination of the MT Ag nanoparticles.

Effect of Reaction Temperature. Solubility and dissociation constant of DDAC to release free Cl^- ions, oxidative capability of NO_3^- ions, and reducing capability of OAm increase with the reaction temperature. As a result, retaining the reaction temperature as high as possible benefits the formation of Ag nanocubes. Images a and b in Figure 4 present TEM images of the samples synthesized at 180 and 220 °C, respectively. The product formed at 180 °C contains MT Ag nanoparticles and single-crystalline AgCl nanoparticles with large size, whose morphologies are changed under irradiation of electron beam in the TEM chamber because of in situ reduction with the electrons (Figure 4a). The result indicates that OAm is not reactive enough to reduce AgCl nanoparticles into single-crystalline Ag polyhedrons at 180 °C. When the reaction temperature increases to 220 °C, the reducing power of OAm is high enough to reduce AgCl nanoparticles, resulting in a product composed of 100% Ag nanoparticles with single-crystalline polyhedrons and MT quasi-spheres (Figure 4b). The coexistence of MT and single crystalline nanoparticles indicates that the combination of Cl^- and NO_3^- ions is still not reactive enough to efficiently etch the MT Ag nanoparticles at this temperature. Once the reaction temperature reaches 260 °C (Figure 1), both reducing power of OAm and oxidative power of the combination of Cl^- and NO_3^- ions can be significantly enhanced to drive the growth of Ag nanocubes in high yield.

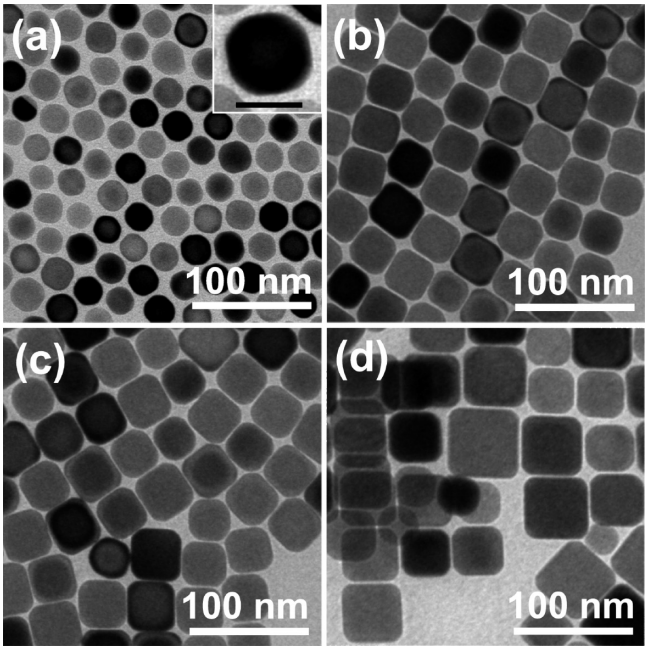

Figure 5. TEM images of single-crystalline Ag nanocubes synthesized by varying the concentration of $AgNO_3$, whereas the molar ratio of DDAC/$AgNO_3$ was maintained at 1.5: (a) 0.002, (b) 0.005, (c) 0.05, and (d) 0.1 M. Other reaction conditions were the same as those of Figure 1. The scale bar in the inset of frame (a) represents 20 nm.

Effect of Concentration of $AgNO_3$. The size of single-crystalline AgCl nanoparticles and the concentration of MT Ag nanoparticles formed at the very beginning of the reactions are strongly dependent on the initial concentration of $AgNO_3$ in the reaction systems. As a result, the dimension of the final Ag nanocubes is expected to be influenced by the concentration of $AgNO_3$. With remaining of the constant molar ratio between DDAC and $AgNO_3$ (i.e., DDAC/$AgNO_3$ = 1.5), the effect of the $AgNO_3$ concentration on the Ag nanoparticles has been investigated and the typical TEM images of the resulting nanoparticles are presented in Figure 5. These images clearly show that the Ag nanoparticles are single crystalline regardless of the $AgNO_3$ concentration in the range of 0.002−0.100 M. Most of the particles have cubic morphology although the particles formed with 0.002 M $AgNO_3$ exhibit relatively high truncation (Figure 5a). The less-cubic morphology highlighted in the inset of Figure 5a might be ascribed to the low concentration of $AgNO_3$ that results MT Ag nanoparticles with a concentration too low to support the growth of the single-crystalline Ag polyhedrons into perfect cubes. Once the concentration of $AgNO_3$ reaches a critical value, i.e., 0.005 M, the shape of the resulting nanoparticles becomes essentially cubic (Figure 5b). Further increase in the concentration of $AgNO_3$ does not change the cubic morphology of the nanoparticles while their size increases accordingly due to the availability of more Ag source. As a result, the size of Ag nanocubes can be tuned in the range of 24−45 nm by simply controlling the concentration of $AgNO_3$ and maintaining a constant molar ratio

(50) Peng, S.; McMahon, J. M.; Schatz, G. C.; Gray, S. K.; Sun, Y. *Proc. Nat. Acad. Sci. U.S.A.* **2010**, *107*, 14530–14534.

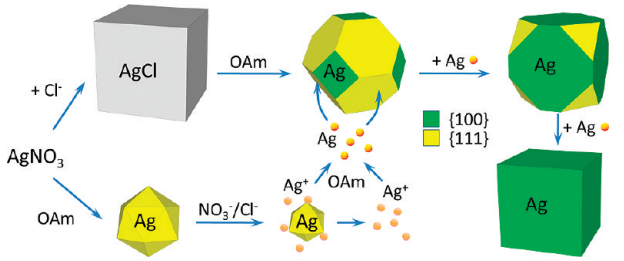

Figure 6. Schematic illustration of the major steps involved in the growth of single-crystalline Ag nanocubes.

(i.e., 1.5) of DDAC/$AgNO_3$ (see the Supporting Information, Figure S9).

Growth Mechanism. Similar to the general rule revealed by the synthesis of shaped nanoparticles in other systems,[2] formation of Ag nanocubes in our present reaction system also involves the sequential nucleation (i.e., formation of single-crystalline seeds) and growth (i.e., slow deposition of Ag atoms on the seeds to enlarge them into cubes with assistance of surfactant) stages according to the experimental results. Figure 6 depicts the major steps involved in evolution of Ag nanocubes when the reaction system is in the presence of high concentration of Cl^- ions. The solution of DDAC in the binary OE−OAm solvent is refluxed at 260 °C to promote the dissociation of DDAC to release a high concentration of Cl^- ions and to increase the reducing capability of OAm. When the solution of $AgNO_3$ is added to the hot DDAC solution, two competitive reactions (i.e., precipitation between Ag^+ ions and Cl^- ions versus fast reduction of Ag^+ ions with hot OAm) instantaneously lead to the formation of both larger single-crystalline AgCl nanoparticles and smaller MT Ag nanoparticles within a couple of seconds. Once free Ag^+ ions are consumed, hot OAm starts to reduce AgCl nanoparticles to transform them into single-crystalline Ag nanoparticles with polyhedral morphologies that are terminated by both {100} and {111} facets. This chemical transformation is also fast and is finished within 1 min. The inheritance of single crystallinity during the transformation from AgCl nanoparticles to Ag ones is not clear yet. The single-crystalline Ag nanoparticles are larger than the MT Ag nanoparticles and exhibit much higher stability. Due to the coexistence of NO_3^- and Cl^- ions in the reaction solution, the MT Ag nanoparticles are not stable enough to resist the oxidative etching,[33] leading to a slow dissolution process with release of Ag^+ ions to the solution. The released Ag^+ ions are then quickly reduced with the hot OAm to form Ag atoms that will condense on the surfaces of the more stable single-crystalline Ag nanoparticles to anisotropically enlarge them into Ag nanocubes. Once the MT nanoparticles are completely etched, the product is dominated by the single-crystalline Ag nanocubes.

Conclusion

In summary, a facile approach has been developed for the successful synthesis of Ag nanocubes with high purity (>95%) and uniform size through reduction of $AgNO_3$ in a binary organic solvent mediated with DDAC that serves as a source to provide free Cl^- ions. Addition of DDAC molecules that are ionized in the binary solvent containing OE is critical to the success in shape selection process because the released Cl^- ions play two important roles (i) reaction with Ag^+ ions ionized from $AgNO_3$ to form single-crystalline AgCl nanoparticles which can be transformed to single crystalline Ag polyhedrons through reduction with OAm; (ii) enhancement in the oxidative etching power of NO_3^- ions to selectively dissolve MT Ag nanoparticles, which are redeposited on the single-crystalline Ag polyhedrons to enlarge them into Ag nanocubes. In addition, the concentration (0.03 M) of DDAC at the optimized reaction conditions is comparable to the concentration (0.02 M) of $AgNO_3$, leading to that the present synthetic strategy is very reliable and repeatable. In contrast, only trace amount of halogenide or chalcogenide is required to mediate the synthesis of Ag nanocubes in hydrophilic solvents and a very small variation in concentration of the additives can drastically influence the quality of the as-synthesized nanoparticles.[31] As a result, the robust synthetic approach presented in our work could be easily scaled up to subgram level mass production of Ag nanocubes with high quality and high purity.

Acknowledgment. We thank Drs. C. Lei and R. Cook for help in TEM characterization. Use of the Center for Nanoscale Materials and the Electron Microscopy Center for Materials Research at Argonne National Laboratory was supported by the U.S. Department of Energy, Office of Science, Office of Basic Energy Sciences, under Contract DE-AC02-06CH11357. TEM and EDS characterization was carried out in part in the Frederick Seitz Materials Research Laboratory Central Facilities, University of Illinois, which are partially supported by the U.S. Department of Energy under grants DE-FG02-07ER46453 and DE-FG02-07ER46471.

Supporting Information Available: Tilted TEM and HRTEM images of the Ag nanocubes; photographs, optical extinction spectra, EDS spectra, and HAADF-STEM images of the samples formed at different times; TEM images of the Ag nanoparticles synthesized in different solvents; and dependence of average size and distribution of Ag nanocubes on the concentration of $AgNO_3$ (PDF). This material is available free of charge via the Internet at http://pubs.acs.org.